Circular Dichroism in the Optical Second-Harmonic Emission of Curved Gold Metal Nanowires

A. Belardini,* M. C. Larciprete, M. Centini, E. Fazio, and C. Sibilia
Dipartimento di Scienze di Base e Applicate per l'Ingegneria, Sapienza Università di Roma and CNISM, Via A. Scarpa 16, I-00161 Roma, Italy

D. Chiappe, C. Martella, A. Toma,† M. Giordano, and F. Buatier de Mongeot
Dipartimento di Fisica, Università di Genova and CNISM, Via Dodecaneso 33, 16146 Genova, Italy
(Received 8 June 2011; published 12 December 2011)

Here we report the experimental observation of circular dichroism in the second-harmonic field (800–400 nm conversion) generated by self-organized gold nanowire arrays with subwavelength periodicity (160 nm). Such circular dichroism, raised by a nonlinear optical extrinsic chirality, is the evident signature of the sample morphology. It arises from the curvature of the self-assembled wires, producing a lack of symmetry at oblique incidence. The results were compared, both in the optical linear and nonlinear regime, with a reference sample composed of straight wires. Despite the weak extrinsic optical chirality of our samples (not observable by our optical linear measurements), high visibility (more than 50%) was obtained in the second-harmonic generated field.

DOI: 10.1103/PhysRevLett.107.257401 PACS numbers: 78.67.Uh, 42.65.Ky, 78.20.Ls, 78.55.−m

Optical second-harmonic generation (SHG) is a very sensitive method for the study of symmetry properties of surfaces and thus was widely used for the characterization of chemical and biological samples [1]. In order to enhance the second-harmonic (SH) conversion efficiency, metal nanopatterned surfaces such as nanoholes [2], nanowires [3,4], and nanorods [5] have been proposed and investigated. In these structures the electric field intensity can increase up to several orders of magnitude due to the mutual effect of field localization near the sharp edges and localized surface plasmon excitation. In this context a great deal of effort was devoted in past years to the study of the linear and nonlinear response of nanopatterned metal surfaces coupled to 3D- [6] or 2D-chiral [7] metamolecules. The importance of chirality, namely, the lack of a plane of symmetry of an object that is nonsuperimposable on its mirror image, arises from different issues. Chiral media can be used in active polarization controllers and light diodes [8] for optical signal processing devices. Moreover, it has recently been shown that nanoscale chiral materials can produce negative refraction [9] and thus can be used as base elements in metamaterial constitution. Apart from 3D- and 2D-chiral objects, the possibility to obtain optical chirality, i.e., optical activity, with nonchiral elements was studied in the past [10], but only recently reconsidered [11–13]. This phenomenon, which can be referred to as optical extrinsic chirality, is obtained when the experimental configuration composed by both the nonchiral object and the optical incident field is nonsuperimposable on its mirror image, and was characterized from the optical linear point of view in Refs. [11–13]. An important result was obtained in Ref. [11] where it was demonstrated that samples showing extrinsic optical chirality can behave as a metamaterial with a negative index of refraction. In this framework characterization of surface chirality of every type (3D, 2D, or extrinsic) by SHG assumes a large interest due to the higher sensitivity with respect to linear optical measurements [14].

Here we use SHG experiments (800–400 nm wavelength conversion) as a powerful tool for evaluating the correlation between the morphology of curved gold nanowire (NW) arrays with subwavelength periodicity (160 nm) and the nonlinear optical activity. The results show a strong extrinsic optical circular dichroism of the SH generated field that depends on the curvature of the wires and their reciprocal orientation with respect to the direction of the impinging light.

Such nanowires were obtained on a glass substrate by a high throughput parallel self-assembling procedure described elsewhere [15] in which ion beam sputtering (IBS) and kinetically controlled deposition [4,16] are combined together. In Fig. 1(a) we show an atomic force microscopy (AFM) topography of an IBS patterned soda lime glass which has been successively employed as a template for the lateral confinement of ordered gold nanowires. The glass substrate was exposed to Ar^+ ion irradiation at the energy of 800 eV and at the angle of 35° measured with respect to the normal (the black arrow represents the projection of the ion beam). After 3 h of exposure, the glass surface developed a regular pattern made up of periodic corrugations whose wave vector is mainly oriented parallel to the ion beam projection; the periodicity was estimated to be around 160 nm by means of the 2D self-correlation function shown in the inset. The AFM pattern evidences that the formed glass ripples tend to form periodic undulations with the concavity facing the ion beam projection. A preliminary analysis reveals that the in-plane radius of curvature R of the undulations is mainly distributed around 400 nm.

 © 2011 American Physical Society

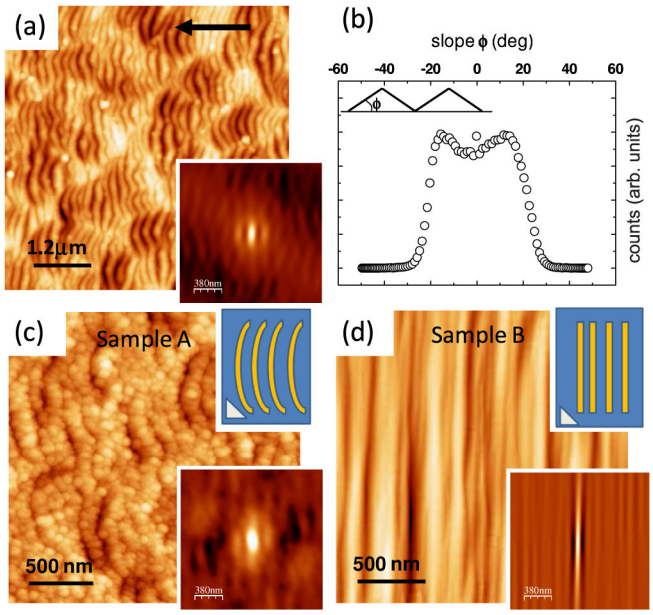

FIG. 1 (color online). (a) AFM morphology of the patterned soda lime glass substrate before Au deposition; the black arrows indicates the ion beam projection. Vertical range of AFM topography: 79 nm. Inset: Autocorrelation of the topographic image, (b) slope distribution of the patterned glass surface of (a) obtained from the first space derivative $dh/dx = h_x$, (c) AFM morphology of sample A (test sample) obtained by glancing angle deposition of Au on the templated glass substrate of (a). Vertical range of AFM topography: 53 nm. Upper inset: Schematic of sample A (the small triangle in one corner of the sample is a reference mark that shows the sample orientation with respect to the fixed external reference). Lower inset: Autocorrelation of the topographic image. (d) AFM morphology of sample B (reference sample, straight nanowires) prepared by direct ion irradiation; vertical range of AFM topography: 83 nm. Upper inset: Schematic of sample B (the small triangle in one corner of the sample is a reference mark that shows the sample orientation with respect to the fixed external reference). Lower inset: Autocorrelation of the topographic image.

Concerning the origin of the curved tracts of the ripples, to our knowledge an accurate investigation on the origin of ripple curvature on glass has so far never been made. In the case of Si, both experimental and theoretical simulations evidence the formation of a characteristic curvature when the ripples get pinned by regions where the density of local defects is higher [17].

The slope distribution of the patterned glass surface is reported in Fig. 1(b): a quasisymmetrical distribution is clearly peaked around $\phi = \pm 15°$, a value that corresponds to the main slope of the ripple sides. In a second stage, Au was thermally evaporated under a grazing incidence condition (75° with respect to the normal) and orthogonally to the ripple structures [the black arrow in Fig. 1(a) also indicates the Au flux direction] in order to localize metal agglomeration in correspondence to the illuminated ripple sides [16]. Under these conditions, the rippled glass substrate, due to shadowing effects, modulates the spatial distribution of the Au flux, inducing the nucleation of metal clusters selectively on the illuminated ridges, where the flux is higher, while the facets on the opposite ripple side remain unexposed to Au. Increasing Au coverage, agglomeration and coarsening of the clusters proceed until a 1D connected polycrystalline Au NW is formed on top of the supporting illuminated ridges. In Fig. 1(c) the AFM image of the produced sample (sample A) shows the presence of a disconnected array of polycrystalline NWs which grow in registry with the glass pattern. More details concerning the growth procedure employed to form this kind of nanowires are provided in Ref. [16], while in Fig. 2(d) of Ref. [4] the optical transmission spectra of sample A is shown. From these experiments we infer that the supporting base of the Au nanowires (corresponding to the ripple illuminated facet) has a width of about 80 nm, while the height of the Au wire measured in the direction orthogonal to the Au facet amounts to about 70 nm.

The use of similar supporting templates prepared by IBS for confining the growth of metal clusters was also discussed in some recent experiments [18–22] which explore a small thickness regime in the range of a few nm, near the percolation threshold. Alternatively, a reference sample which presents a disconnected array of straight wires has been prepared recurring to direct ion beam irradiation of a polycrystalline Au film supported on a flat glass template [sample B in Fig. 1(d)]. The growth and morphology of this sample have been described in detail in Refs. [23,24] while the optical transmission spectra of sample B have been shown in Fig. 3(c) of Ref. [4].

For both samples A and B the nanowires are laterally disconnected in the direction orthogonal to the ridges (see the morphological analysis presented in Refs. [16,25]); conversely, in the parallel direction they form chains of interconnected grains which can reach the length of several micrometers. The strong dichroism in the optical transmission spectra confirms the morphological anisotropy of the nanowires. In particular, for light polarized in the transverse direction, the excitation of localized plasmon resonances induces a clear extinction maximum, while for light polarized in the longitudinal direction no localized plasmon extinction can be found, and the spectra resemble those of a continuous connected film.

Optical linear and nonlinear transmission measurements were performed both on the test sample (sample A) and on the reference sample (sample B) with the same input laser and similar setups. The size of both samples is 1×1 cm^2. The input light source is a pulsed Ti:sapphire laser with either right-handed or left-handed circular polarized light (the choice depends on the orientation of a $\lambda/4$ plate). The light (with 150 fs of pulse duration, wavelength of 800 nm, repetition rate of 1 kHz, pulse intensity of 2.4 GW/cm^2) impinges on the sample with a spot diameter of 3 mm at different incidence angles α. The out-coming light is then filtered by an analyzer that can be set for either

p- or s-polarization transmission and then is sent either on a photodiode (in the case of linear measurements) or to a filtered (< 450 nm wavelength) photomultiplier (in the case of nonlinear measurements). The results of the measurements are expressed in a dimensionless form [1,26,27]: linear optical circular dichroism (CD) is the difference between the transmitted intensity (at the s- or p-polarization state) of the left-handed circular polarized light and the right-handed one divided by the average total intensity:

$$\mathrm{CD} = \frac{I_L^\omega - I_R^\omega}{(I_L^\omega + I_R^\omega)/2}; \tag{1}$$

meanwhile, the nonlinear optical circular dichroism (SHGCD) is the difference between the generated SH field intensity (at the s- or p-polarization state) obtained from the left-handed circular polarized light and the right-handed one divided by the average total generated intensity:

$$\mathrm{SHGCD} = \frac{I_L^{2\omega} - I_R^{2\omega}}{(I_L^{2\omega} + I_R^{2\omega})/2}. \tag{2}$$

In Fig. 2 the results of the linear optical measurements (p-polarized output light) are shown: neither the reference sample with straight wires nor the test sample with curved wires exhibit any circular dichroism in the limit of the setup sensitivity. In both cases the measurements were repeated with samples rotated of 180° around the normal to the surface direction as shown in the figure. In Fig. 3

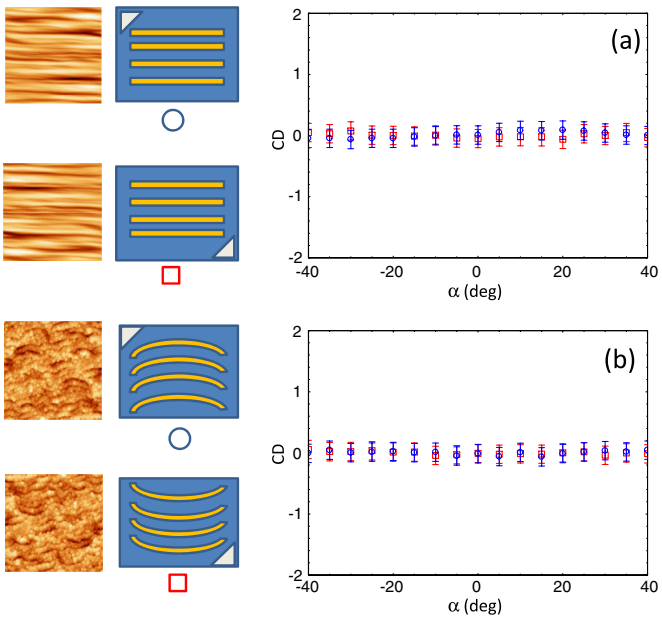

FIG. 2 (color online). Optical linear measurements. (a) Optical circular dichroism (CD) of sample B as a function of the incidence angle (α) for an orientation of the sample (blue circles) with horizontal wires, and with the sample turned upside down by a 180° rotation (red squares). (b) CD of sample A for an orientation of the sample (blue circles) with the center of curvature pointing down, and with the sample turned upside down by a 180° rotation (red squares), so the center of curvature is pointing up. On the left-hand side: Schematics of the samples with the corresponding marks in the measurements (blue circle or red square).

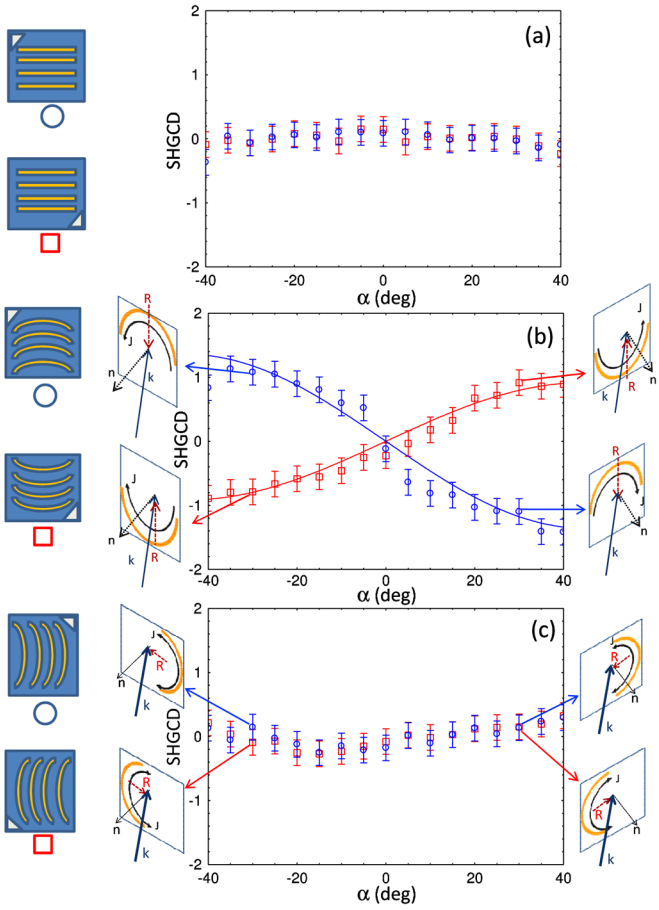

FIG. 3 (color online). Nonlinear optical measurements. First column: Schematics of the samples with the corresponding marks in the measurements (blue circle or red square). Second column: Schematics of the orientation of sample A for negative incidences angle are shown together with the direction of $\hat{k}$ (solid blue arrow), $\hat{n}$ (dotted black arrow), $\hat{R}$ (dashed red arrow), and the preferential direction of the induced current density J (curved black arrow). In the third column are reported the nonlinear optical measurements: (a) SHGCD of sample B for an orientation of the sample (blue circles) with horizontal wires, and with the sample turned upside down by a 180° rotation (red squares); (b) SHGCD of sample A for an orientation of the sample (blue circles) with the center of curvature pointing down, and with the sample turned upside down by a 180° rotation (red squares), so with the center of curvature pointing up. The two lines are the fitting curves as defined by formula (6); (c) SHGCD of sample A for an orientation of the sample (blue circles) with the center of curvature pointing left, and with the sample turned upside down by a 180° rotation (red squares), so with the center of curvature pointing right. In the fourth column the schematics of the orientation of sample A for positive incidence angles are shown together with the direction of $\hat{k}$ (solid blue arrow), $\hat{n}$ (dotted black arrow), $\hat{R}$ (dashed red arrow) and the preferential direction of the induced current density J (curved black arrow).

the results for the nonlinear optical measurements (p-polarized output light) are reported: nonlinear circular dichroism is not observed from the reference sample [Fig. 3(a)]; meanwhile, the test samples exhibit an extraordinarily large SHGCD with 54% of visibility (VIS) [Fig. 3(b)], where the visibility is considered to be

$$\mathrm{VIS} = \frac{\max_{\mathrm{meas}} - \min_{\mathrm{meas}}}{\max_{\mathrm{theor}} - \min_{\mathrm{theor}}} = \frac{\max_{\mathrm{meas}} - \min_{\mathrm{meas}}}{4}. \quad (3)$$

In the case of the radius of curvature of the NWs facing down [blue circles in Fig. 3(b)], for negative incidence angles the extrinsic chirality leads to a larger SH conversion with left-handed circular polarized pump field, while for positive angles the sign of extrinsic chirality changes and the nonlinear response is stronger when a right-handed polarized pump field is considered. Rotating sample A by 180° with respect the normal to the surface results in a sign inversion of the extrinsic chirality (due to the change of sign of the curvature of the wires) and, as expected, the measurements show an inverted trend with respect to the previous case [see red squares in Fig. 3(b)]. This phenomenon of the inversion of the measurements trend by a rotation of 180° around $\hat{n}$ guarantees that the chiral effect we are observing is really due to the curvature of the wires ($\hat{R}$ changes the sign by a 180° rotation) rather than the mere effect of the chirality of the experimental setup. As a further test for the geometry induced chirality, the same measurements where repeated with the curved wires mainly aligned along the sample rotation axis. In this case the curvature of the wires lies on the incidence plane (the plane defined by the normal at sample surface and the direction of light) and no chiral effect is present [Fig. 3(c)]. The nonlinear optical measurements obtained for s-polarized output light are similar to the case of p-polarized light, but we report a lower visibility (17%) due to a lower signal to noise ratio. Indeed, in the measurements showing chirality (where the wires are mainly oriented along the horizontal direction), the p polarization corresponds to the long direction of the wires while the s polarization corresponds to the short direction. Thus the nonlinear polarization vector has a larger component along the direction of the wires leading to a higher p-polarized SHG signal.

The measurements highlight (as expected from the theory [11]) that extrinsic optical chirality arises when the wave vector direction $\hat{k}$, the normal to the sample surface $\hat{n}$, and the direction of the curvature $\hat{R}$ do not lie on the same plane (i.e., they form a nonplanar triad). The handedness of the chirality can be related to the sign of the "extrinsic optical chirality" (EXCH) expression:

$$\mathrm{EXCH} = \frac{1}{R}\hat{R} \cdot \hat{k} \times \hat{n}. \quad (4)$$

The positive (negative) sign indicates a right-handed (left-handed) triad, zero stands for a nonchiral triad. The choice to make explicit in formula (4) the dependence on the curvature $1/R$ (where R is the radius of curvature of the wires and the $\hat{R}$ is the average direction of the radii of curvature) was made in order to cancel the product in the case of straight wires; in this case the surface of the sample lacks any polar orientation as confirmed by the measurements in Fig. 3(a). It is worth noting that the product (4) can also vanish when the light impinges on the sample at normal incidence [see the measurements in Fig. 3(b) when $\alpha = 0$] or when the sample is oriented with the curvature direction lying in the plane of incidence [see the measurements in Fig. 3(c) for every α].

From the nonlinear optical point of view the SH signal is generated from the wires mainly by the magnetic dipole term or Lorentz term [4,28,29]

$$\vec{P}_{2\omega} = \frac{e}{m\omega}\left(\frac{i}{2i\omega - \gamma_{2\omega}}\right)\vec{J}_{\omega} \times \vec{B}_{\omega}, \quad (5)$$

where e is the modulus of the electron charge, m is the electron effective mass, and γ is a damping coefficient taking into account Ohmic losses. When the light impinges on a tilted sample with the radius of curvature pointing down and with negative angles, the curved wire can be seen as an element of a conductive left-handed helical coil providing a preferential path for the induced electronic current density J. Thus, the SH signal shows a larger generation when it is excited by a left-handed circularly polarized light. On the other hand, if the tilting incidence angle is of the opposite sign [i.e., the vectorial product $\hat{k} \times \hat{n}$ in formula (3) changes the sign], the right-handed circularly polarized pump produces a larger SH signal [blue circles in Fig. 3(b)].

The situation is reversed when the sample is rotated by 180° [i.e., the radius of curvature direction changes the sign], changing the sign in expression (4) leading to an inverted behavior in the measurements [red squares in Fig. 3(b)].

Finally, our analysis leads to the conclusion that higher SHG efficiency is achieved when there is concordance between the sign of the geometrical extrinsic chiral EXCH term in formula (4) and the sign used to identify angular momentum or "spin" of the circularly polarized light [$+1$ (-1) for right-handed (left-handed) polarization].

The overall SHGCD signal can be fitted by a phenomenological expression:

$$\begin{aligned}\mathrm{SHGCD} &= \mathrm{const}\frac{1}{R}\hat{R} \cdot (\hat{k} \times \hat{n})\frac{P_{\omega}^2}{A}\cos(\alpha) \\ &= \mathrm{const}\frac{1}{R}\hat{R} \cdot (\hat{k} \times \hat{n})\frac{P_{\omega}^2}{A}(\hat{k} \cdot \hat{n}), \end{aligned} \quad (6)$$

where P_{ω} is the input power at the fundamental angular frequency ω, A is the spot size area, and const is a suitable fitting constant. The $\frac{P_{\omega}^2}{A}\cos(\alpha) = \frac{P_{\omega}^2}{A}(\hat{k} \cdot \hat{n})$ term accounts

for the enlargement of the spot size when the light impinges out of the normal incidence ($\alpha \neq 0$).

In Fig. 3(b) the measurements are reported together with the fitting curves.

In conclusion, we present the evidence of huge extrinsic optical activity in curved gold nanowires. It is remarkable that, due to the beam or structure geometry, the achiral structure of curved nanowires is made to behave efficiently like a chiral medium in the second-harmonic field. More than 50% of visibility was obtained by exploiting the extrinsic optical chirality in the second-harmonic regime, an extraordinary results if compared with the vanishing contrast obtained in the linear optical regime at the same conditions. The strong visibility of the chiral signal together with the low-cost self-assembling procedure are promising issues for developing novel nanoscale electromagnetic devices for active polarization controllers such as rotators and modulators and possible metamaterials.

The authors gratefully acknowledge L. Di Dio and G. Leahu for experimental support. This work was financially supported by PRIN programme. F. B. d. M acknowledges support from Fondazione Carige and ENEA under project MSE.

*Corresponding author.
alessandro.belardini@uniroma1.it
†Present address: Nanobiotech Facility, Istituto Italiano di Tecnologia, via Morego 30, Genova, I-16163, Italy.

[1] T. Verbiest, K. Clays, V. Rodriguez, *Second-Order Nonlinear Optical Characterization Techniques* (CRC Press, New York, 2009).
[2] J. A. H. van Nieuwstadt, M. Sandtke, R. H. Harmsen, F. B. Segerink, J. C. Prangsma, S. Enoch, and L. Kuipers, Phys. Rev. Lett. **97**, 146102 (2006).
[3] T. Kitahara, A. Sugawara, H. Sano, and G. Mizutani, J. Appl. Phys. **95**, 5002 (2004).
[4] A. Belardini, M. C. Larciprete, M. Centini, E. Fazio, C. Sibilia, M. Bertolotti, A. Toma, D. Chiappe, and F. Buatier de Mongeot, Opt. Express **17**, 3603 (2009).
[5] C. Hubert, L. Billot, P.-M. Adam, R. Bachelot, P. Royer, J. Grand, D. Gindre, K. D. Dorkenoo, and A. Fort, Appl. Phys. Lett. **90**, 181105 (2007).
[6] J. K. Gansel, M. Thiel, M. S. Rill, M. Decker, K. Bade, V. Saile, G. von Freymann, S. Linden, and M. Wegener, Science **325**, 1513 (2009).
[7] V. K. Valev, A. V. Silhanek, N. Verellen, W. Gillijns, P. Van Dorpe, O. A. Aktsipetrov, G. A. E. Vandenbosch, V. V. Moshchalkov, and T. Verbiest, Phys. Rev. Lett. **104**, 127401 (2010).
[8] B. J. Broughton, M. J. Clarke, A. E. Blatch, and H. J. Coles, J. Appl. Phys. **98**, 034109 (2005).
[9] J. B. Pendry, Science **306**, 1353 (2004).
[10] R. Williams, Phys. Rev. Lett. **21**, 342 (1968).
[11] E. Plum, X.-X. Liu, V. A. Fedotov, Y. Chen, D. P. Tsai, and N. I. Zheludev, Phys. Rev. Lett. **102**, 113902 (2009).
[12] S. N. Volkov, K. Dolgaleva, R. W. Boyd, K. Jefimovs, J. Turunen, Y. Svirko, B. K. Canfield, and M. Kauranen, Phys. Rev. A **79**, 043819 (2009).
[13] S. V. Zhukovsky, C. Kremers, and D. N. Chigrin, arXiv:1103.5008v1.
[14] T. Verbiest, M. Kauranen, A. Persoons, M. Ikonen, J. Kurkela, and H. Lemmetyinen, J. Am. Chem. Soc. **116**, 9203 (1994).
[15] U. Valbusa, C. Boragno, and F. Buatier de Mongeot, Mater. Sci. Eng., C **23**, 201 (2003).
[16] A. Toma, D. Chiappe, D. Massabò, C. Boragno, and F. Buatier de Mongeot, Appl. Phys. Lett. **93**, 163104 (2008).
[17] A. Keller, S. Facsko, and W. Moller, New J. Phys. **10**, 063004 (2008).
[18] M. Ranjan, T. W. H. Oates, S. Facsko, and W. Möller, Opt. Lett. **35**, 2576 (2010).
[19] S. Numazawa, M. Ranjan, K.-H. Heinig, S. Facsko, and R. Smith, J. Phys. Condens. Matter **23**, 222203 (2011).
[20] S. Camelio, D. Babonneau, D. Lantiat, L. Simonot, and F. Pailloux, Phys. Rev. B **80**, 155434 (2009).
[21] D. Babonneau, S. Camelio, L. Simonot, F. Pailloux, P. Guérin, B. Lamongie, and O. Lyon, Europhys. Lett. **93**, 26 005 (2011).
[22] J.-H. Kim, N.-B. Ha, J.-S. Kim, M. Joe, K.-R. Lee, and R. Cuerno, Nanotechnology **22**, 285301 (2011).
[23] A. Toma, D. Chiappe, B. Šetina Batič, M. Godec, M. Jenko, and F. Buatier de Mongeot, Phys. Rev. B **78**, 153406 (2008).
[24] A. Toma, B. Šetina Batič, D. Chiappe, C. Boragno, U. Valbusa, M. Godec, M. Jenko, and F. Buatier de Mongeot, J. Appl. Phys. **104**, 104313 (2008).
[25] A. Toma, D. Chiappe, C. Boragno, and F. Buatier de Mongeot, Phys. Rev. B **81**, 165436 (2010).
[26] T. Petralli-Mallow, T. M. Wong, J. D. Byers, H. I. Yee, and J. M. Hicks, J. Phys. Chem. **97**, 1383 (1993).
[27] J. J. Maki, M. Kauranen, and A. Persoons, Phys. Rev. B **51**, 1425 (1995).
[28] M. Centini, A. Benedetti, C. Sibilia, and M. Bertolotti, Opt. Express **19**, 8218 (2011).
[29] M. C. Larciprete, A. Belardini, M. G. Cappeddu, D. de Ceglia, M. Centini, E. Fazio, C. Sibilia, M. J. Bloemer, and M. Scalora, Phys. Rev. A **77**, 013809 (2008).